ROBUST IMPLEMENTATION OF MVA BY DOUBLE PATH-INTEGRAL MIGRATION

R. G. Bedendo, J. Schleicher, and J. C. Costa

email: *js@ime.unicamp.br*

keywords: *Velocity Analysis, Imaging, Coherency Measure, Multi-Stack, Migration*

ABSTRACT

Path-integral migration is a method for creating a migrated image without previous knowledge of the true velocity model by summing the migrated images from a representative set of velocity models. This concept can be expanded to automatically extract a velocity model, a technic called Migration Velocity Analysis by Double Path-Integral Migration (MVA by DPIM). In MVA by DPIM, a second, weighted image is created, with the weight containing the velocities used in the individual migrations. Division of the two images provides the velocity model. Here we discuss several practical aspects of implementing MVA by DPIM, ranging from the parametrization of the weight function to the stabilization of the division and the selection of only meaningful velocities. By means of tests on a wide range of velocity models, we find a robust implementation of the method.

INTRODUCTION

Path-integral migration (PIM) is a method for creating a migrated image without previous knowledge of the true velocity model (Landa, 2004; Landa et al., 2006). This image is contructed by summing the migrated images from a representative set of velocity models. This concept can be expanded to automatically extract a velocity model, a technic which we refer to as Migration Velocity Analysis by Double Path-Integral Migration (MVA by DPIM) (Schleicher and Costa, 2009; Costa and Schleicher, 2011). In this method, two images are created. The first one is the one generated in basic PIM, the second one is a weighted image, in which the weights contain the velocities used in the individual migrations prior to stacking. The velocity model is then obtained by the division of the two images.

The basic idea of generating images without knowledge of the necessary parameters was introduced by Keydar (2004) for homeomorphic imaging and by Landa (2004) for migration. Since it is conceptually similar to the path-integral formulation of quantum mechanics (Feynman and Hibbs, 1965), Landa (2004) referred to it as "path-summation migration" and Landa et al. (2006) used the term "path-integral seismic imaging".

Landa et al. (2006) discuss PIM in more detail. They argue that for the method to be successful, three conditions should be satisfied:

- The integration should be carried out over a representative set of all possible trajectories, that is, the set of velocity models used for migrating the data prior to stacking should be a good representation of all the possible velocity models.
- An appropriate weight function should be used, containing some sort of coherency measure (such as semblance, flatness of common-image gahters, etc.), in order to help the procedure converge to the proper image, by means of reinforcing the focused and penalizing unfocused contributions.
- The path-integral argument should be chosen properly, specifically the phase function for a real or complex-valued exponential.

The original formulation of PIM replaces the complex optimization process of velocity-model building with a summation over "all possible trajectories", that is, stacking the images of a representative set of all possible velocity models. In this way, a seismic image can be created with minimal to none human intervention. Keydar (2004) and Landa (2004) proposed the use of path-integral-like concepts in seismic imaging in order to overcome the strong dependency of the seismic image on the knowledge of a high-quality velocity model. In theory, PIM should be able to focus an image even in regions where conflicting velocity information would be necessary to do so.

However, a migration-velocity model is not only desirable to construct a seismic image, but is also the input for more more refined methods, such as Tomography (Billette et al., 2003; Clapp et al., 2004), Joint Migration/Inversion (Berkhout, 2014), or Full Waveform Inversion (Virieux and Operto, 2009).

Therefore, Schleicher and Costa (2009) proposed a method to extract an associated velocity model by combining path-integral imaging with the method for extracting additional parameters from double stacking in Kirchhoff migration as discussed by Bleistein (1987) and Tygel et al. (1993). Schleicher and Costa (2009) used data from Born modeling in a smoothed version of the Marmousi model (Billette et al., 2003). Their choice of the coherency measure was the squared average of the absolute value of the local event slopes in the common-image gather (CIG), and the weight function was a real valued exponential containing the coherency measure. Costa and Schleicher (2011) demonstrated the use of MVA by DPIM using this coherency measure for a real seismic data set. However, they had to come up with some stabilization that were specific to that data set to make the method work for real data.

In this work we test other parametrizations of the coherency measure and weight function in MVA by DPIM on synthetic data from a wide range of velocity models so as to improve the stability of the method in different situations. Some of the situations analyzed include:

- presence of random noise, with varying signal-to-noise ratios;
- linear variation of velocity, horizontally and with depth;
- different wavelet signatures, including Ricker (various peak frequencies).

These tests allow us to find a more stable implementation of MVA by DPIM which works on a wide range of data sets.

MVA BY DPIM

Path integral migration (PIM)

Let us denote the vertical (one-way) time by τ and the lateral distance by x. Then, the basic operation of path-integral time migration at each image point $\mathbf{x} = (x, \tau)$ can be represented, using a similar notation to Landa et al. (2006), as

$$V_\beta(\mathbf{x}) = \int d\alpha \, w_\beta(\mathbf{x}, \alpha) Q(\mathbf{x}, \alpha) \, , \tag{1}$$

where $Q(\mathbf{x}, \alpha)$ is a single migrated image for a certain velocity model parameterized by α, and the variable w_β denotes a weight function, which is a function of $\mathbf{x}$ and α. In other words, V_β is the stack over all migrated images at $\mathbf{x}$ for all migration velocity models (or "paths") under consideration. For Kirchhoff time migration as considered here, Q is given by

$$Q(\mathbf{x}, \alpha) = \int dh \int d\xi \int dt \, U(t, \xi, h) \delta(t - t_d(\xi, \mathbf{x}, h; \alpha)) \, , \tag{2}$$

where $U(t, \xi, h)$ is the seismic trace recorded at midpoint ξ and half-offset h, and $t_d(\xi, \mathbf{x}, h; \alpha)$ is the set of stacking surfaces corresponding to set of the velocity models under consideration.

In the most general interpretation of the above equations, α is a set o parameters that define the velocity models. In the context of time-migration MVA by DPIM, α can be chosen to simply represent the value of the migration velocity. In principle, α could be a function of $\mathbf{x}$, but in this work the set of velocity models used in the migrations prior to stacking includes only constant velocity models.

Weight function

In its basic form, the weight w_β in expression expression (1) is defined as

$$w_\beta(\mathbf{x}, \alpha) \; = \beta \, \exp \, \left[-C(\mathbf{x}, \alpha) \, / \, \sigma^2 \right] \; , \tag{3}$$

where $C(\mathbf{x}, \alpha)$ is a nonnegative number that increases with decaying quality of the image at point **x**, and σ is a parameter that controls the decay of the weight function as image quality decreases. Landa et al. (2006) propose to make use of a coherency measure in the migrated CIG at **x** to define C. Schleicher and Costa (2009) make use of the fact that for a good image, the events in CIGs should be flat, i.e., they should present vanishing event slopes p. Therefore, they used, at each image point $\mathbf{x} = (x, \tau)$, the squared average of the absolute value of the local event slopes p along horizontal lines in the CIG at x to calculate the quality measure $C(\mathbf{x}, \alpha)$.

Double path-integral migration (DPIM)

In DPIM, the stacking operation defined by expression (1) is carried out with different weight functions w_β. The difference between the weights is in the value of parameter β. For the basic image, $V_1(\mathbf{x})$, it is chosen as $\beta = 1$. For the second image, the weight includes a factor to account for the velocity value used in each migration prior to stacking, i.e., $\beta = \alpha$, resulting in a velocity weighted image $V_\alpha(\mathbf{x}$.

Using Laplace's method (Erdélyi, 1956), the integral in (1) with the weight functions defined as according to equation (3) can be evaluated as

$$V_\beta(\mathbf{x}) \; \approx \; \beta_0 \sqrt{\frac{2\pi \; \sigma^2}{C''(\mathbf{x}, \alpha_0)}} \, Q_0(\mathbf{x}, \alpha_0) \tag{4}$$

where $\alpha_0 \; = \; \alpha_0(\mathbf{x})$ is the stationary value of α at image point **x**, $C''(\mathbf{x}, \alpha_0)$ is the second derivative of the quality measure C with respect to α, taken at α_0, and $Q_0(\mathbf{x}, \alpha_0)$ is the stationary migrated image for velocity distribution $\alpha_0(\mathbf{x})$, the image where the reflectors come into focus.

Equation (4) shows that PIM provides an image that is directly proportional to the focused migrated image, with β_0 denoting the stationary value of factor β. Because of the chosen values for β, we have for the first image $V_1(\mathbf{x})$, $\beta_0 = 1$ and for the second image, $V_\alpha(\mathbf{x})$, $\beta_0 = \alpha_0$.

Since the two results (1) and (4) differ only by a factor α_0, the (stationary) velocity model can be extracted by the division of the two images, viz.,

$$\alpha_0(\mathbf{x}) \; = \; \frac{V_\alpha(\mathbf{x})}{V_1(\mathbf{x})} \; . \tag{5}$$

Of course, the division of two seismic images creates some stability issues which need to be taken care of. In this paper, we discuss several ideas that help to ensure that the procedure to extract a velocity model is robust in most practical situations.

ROBUST VELOCITY EXTRACTION

Masked division

Schleicher and Costa (2009) tested different ways of performing the division of the images, such as stabilized division and masked division. They discarded stabilized division because it alters the extracted velocity values. In their masked division, they only accept the results of division (5) at nodes (image points) where

$$v_{min} \; < \; \alpha_0(\mathbf{x}) \; < \; v_{max} \; , \tag{6}$$

where v_{min} and v_{max} are, respectively, the minimum and maximum values of the set of velocities used in the migrations prior to stacking. They also discussed methods to fill the created model where the division was considered faulty or couldn't be performed (nearest-neighbour filling, moving average smoothing, B-splines smoothing). Their choices (masked division and B-splines smoothing) were tested successfully on real data by Costa and Schleicher (2011).

However, for the real-data example, they had to make some choices that are not immediately applicable to other data sets. Therefore, the need arose to look for more general solutions to the stability issues. Below, we discuss three additional measures that help to stabilize MVA by DPIM.

Energy cut

Because of the success of masked division in the original papers, but some difficulties in other tests, particularly involving noisy data, we tested in this work a slightly more sophisticated version of masked division that tries to take the noise level into account. Our implementation uses two amplitude values: the maximum (E_{max}) and minimum (E_{min}) average value of the data energy in a time window (250 ms in our numerical tests), as computed over all possible such windows in the entire stacked image V_1 of equation (1). With these reference values, we define a threshold value as

$$E_{cut} \;=\; E_{min} \;+\; \zeta(E_{max} - E_{min}) \tag{7}$$

where ζ is a factor between zero and one, choosing a certain percentage of the diference between E_{max} and E_{min}. In this way, we find two additional criteria for accepting the result of division (5) at $\mathbf{x}$, being

$$V_1(\mathbf{x}) \;>\; E_{cut}\;, \tag{8}$$

$$V_\alpha(\mathbf{x}) \;>\; \alpha E_{cut}\;. \tag{9}$$

Weight map

As another additional measure to help evaluating the validity of the extracted velocity model, we create a third image, using an additional weight with $\beta = w_1$, i.e., using the weight function

$$w_w(\mathbf{x},\alpha) \;=\; (\exp\,\left[-C(\mathbf{x},\alpha)\,/\,\sigma^2\right])^2 \tag{10}$$

in equation (1). As with the two previous weight functions, the integral in (1) with this weight function (10) can be evaluated as

$$V_w(\mathbf{x}) \;\approx\; w_0\,\sqrt{\frac{2\pi\sigma^2}{C''(\alpha_0)}}\,Q_0(\mathbf{x},\alpha_0)\;, \tag{11}$$

where w_0 denotes the stationary value of the original weight function w_1 at $\mathbf{x}$. Therefore, the image V_w can be used to extract a map of these stationary values of the weight function by means of dividing image (11) by the first image, (1), to obtain

$$w_0(\mathbf{x}) \;=\; \frac{V_w(\mathbf{x})}{V_1(\mathbf{x})} \tag{12}$$

Of course, the division in equation (12) is carried out only if V_1 makes the energy cut.

We use the resulting weigh map to validate the velocity model created by the division in equation (5), that is, velocities are accepted only at nodes where the weight calculated by (12) is above a certain threshold, i.e.,

$$w_0(\mathbf{x}) \;>\; w_{min}\;, \tag{13}$$

where w_{min} is a chosen parameter threshold for the auxiliary map $w_0(\mathbf{x})$.

Quality measure

The weight function in equation (3) makes use of a quality measure of the image $Q(\mathbf{x},\alpha)$ at $\mathbf{x}$. Schleicher and Costa (2009) used, at each image point $\mathbf{x} = (x,\tau)$, the squared average of the absolute value of the local event slopes p along horizontal lines in the CIG at x to calculate this measure. Here, we propose to use an offset-weighted average over the squared slopes as a slightly modified quality measure that helps to increase robustness.

Denoting the CIG at lateral position x after migration with velocity α by $\psi(h, \tau; x, \alpha)$, the local event slope $p(h_k, \tau_l; x, \alpha)$ at a point (h_k, τ_l) in the CIG can be determined according to Schleicher et al. (2009) as

$$p(h_k, \tau_l; x, \alpha) \;=\; s \sqrt{\frac{\sum_{(ij)\in W_{kl}} (\psi_x(h_i, \tau_j; x, \alpha))^2}{\sum_{(ij)\in W_{kl}} (\psi_t(h_i, \tau_j; x, \alpha))^2}} \;, \tag{14}$$

with $s = s(h_k, \tau_l; h, \alpha)$ given by

$$s \;=\; -\mathrm{sgn} \left(\sum_{(ij)\in W_{kl}} \psi_x(h_i, \tau_j; x, \alpha) \psi_t(h_i, \tau_j; x, \alpha) \right) \;. \tag{15}$$

In (14) and (15), W_{kl} denotes a selected window of size $2I + 1 \times 2J + 1$ centered at (h_k, τ_l) within the CIG, i.e.,

$$W_{kl} = \{i, j \mid k - I \leq i \leq k + I,\; l - J \leq l \leq l + J\} \;. \tag{16}$$

Moreover, $\psi_x(h_i, \tau_j; x, \alpha)$ and $\psi_t(h_i, \tau_j; x, \alpha)$ are the discretized values of the horizontal and vertical derivatives of ψ calculated at $(x_i, \tau_j) \in W_{kl}$.

After applying an automatic gain control (AGC) to the data migrated with a certain velocity α, we calculate $C(\mathbf{x}, \alpha)$ by means of an offset-weighted average according to

$$C(\mathbf{x}, \alpha) \;=\; \frac{\sum_{i=1}^{nh} p^2(h_i, \tau; x, \alpha) \bar{h}_i^2}{\sum_{i=1}^{nh} \bar{h}_i^2} \;, \tag{17}$$

where nh represents the number of nonmuted offsets in the CIG at vertical time τ, and where $\bar{h}_i = \bar{h}_i(x, \tau) = h_i / h_{max}(x, \tau)$ with h_{max} denoting the maximum nonmuted offset.

The weights in average (17) are used so as to reinforce the values of the coherency calculated at larger offsets, thus increasing the sensitivity to velocity errors.

Coherency measure

Even with the improved quality measure of equation (17), additional care needs to be taken if the maximum usable offsets is rather small. In that case, the events in the CIG are almost flat for a relatively large interval of velocities, leading to low C values (indicating high quality). Another caution regarding the quality map of equation (17) is that it can fail to identify random noise from real data, that is, it may calculate rather low C values for random noise.

To correct for these problems, we have included a second coherency measure into the procedure. Our choice in this case is the traditional semblance (Neidell, 1971),

$$S(h_k, \tau_l; x, \alpha) = \frac{\sum_j (\sum_i \psi(h_i, \tau_j; x, \alpha))^2}{(2I + 1) \sum_j \sum_i (\psi(h_i, \tau_j; x, \alpha))^2} \;, \tag{18}$$

calculated in the same window as the slope p. This second measure is used as to define a threshold S_{min} for accepting the value of p in the average calculation of equation (17). In other words, the weights $\bar{h}_i$ are modified to

$$\bar{h}_i = \begin{cases} h_i / h_{max}(x, \tau) & S(h_i, \tau; x, \alpha) > S_{min}, \\ 0 & \text{else.} \end{cases} \tag{19}$$

Model building

At all nodes **x** where at least one of the above conditions (6), (8), (9), or (13) is not satisfied, the values of V_α and V_w are set to zero.

After the division masked in this way, we apply a a trapezoidal filter to the created model, designed to remove boundary effects, and a median filter to remove very strong local variations of velocity. Finally, a routine for B-spline interpolation and smoothing fills all gaps in the velocity model. The B-splines

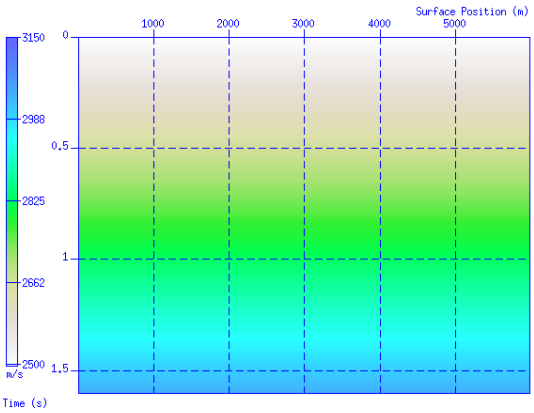

Figure 1: Example 1: Model used to generate the synthetic data.

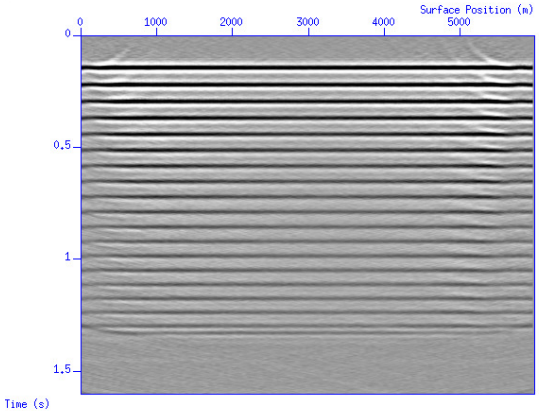

Figure 2: Example 1: Stacked image created without weight.

coeficients are calculated by regularized least squares. The intensity of the smoothing applied is another parameter that must be carefully selected.

Our numerical tests have shown that in this way, incorrect division results are quite reliably eliminated. The remaining reliable velocity values are sufficient to build a meaningful time-migration velocity model.

NUMERICAL EXAMPLES

Input sets of velocity models

Selecting a proper set of velocity models to be used in the migrations prior to stacking is the first step for testing the implementation of the method. For the choice of such a set, the desired quality of the model to be extracted by this technique must be weighted against the required computer time. Since in time migration, the velocities at different image points are independent of each other, we considered in all our numerical tests only sets of constant velocity models. For the stationarity principle to work, the stationary values must not fall close to the integration limits. Therefore, we considered sets with a lowest velocity value of 1200 m/s and highest value of 4000 m/s, with different values for the velocity increase between migrations. For each value in the set of input velocities, we carry out common-offset Kirchhoff time migrations, resulting in a data cube $\psi(\mathbf{x}, h, \alpha)$, with h being the half offset.

Example 1: Vertical-gradient model

As our reference model while developing our robust implementation, we used synthetic data from a model with 20 horizontal reflectors embedded in a varying-velocity background (see Figure 1). In this example, the velocity varies linearly from 2500 m/s at the top increasing by 200 m/s at each 1000 m in depth. Therefore, at the deepest reflector at 5 km depth, the velocity reaches 3600 m/s. We simulated multicoverage seismic data using the **SUSYNLV** routine of Seismic Unix with 117 sources between $x = 0$ km and 5.85 km, spaced at 50 m, using 120 receivers in each common-shot gather, spaced at 25 m. The peak frequency of the Ricker wavelet is 12 Hz. To these data, we added random noise with a signal-to-noise ratio of 10 using the **SUADDNOISE** routine of Seismic Unix.

For the multiple migrations in the path-integral approach, we used constant-velocity models (set of velocity models used for migrating the data prior to stacking) starting at $v_{min} = 1200$ m/s and ending at $v_{max} = 4000$ m/s. In the first test, we increased the migration velocity by 50 m/s for each migration. Figure 2 exhibits the stack of migrated images obtained without any weight function ($w = 1$) in equation (1).

Figure 3 shows the first image generated by the routine, corresponding to the stacked values of the images migrated with weight function (3) with $\beta = 1$. Similarly, Figure 4 shows the image obtained by stacking the migrated images with weight function (3) with $\beta = \alpha$. In both figures, we observe the

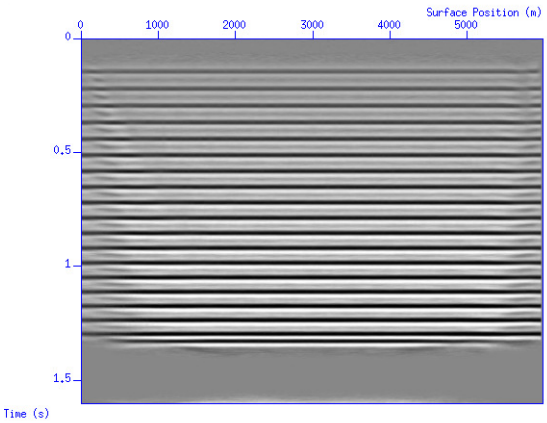

Figure 3: Example 1: Stacked image generated with weight function (3) (PIM, $\beta = 1$).

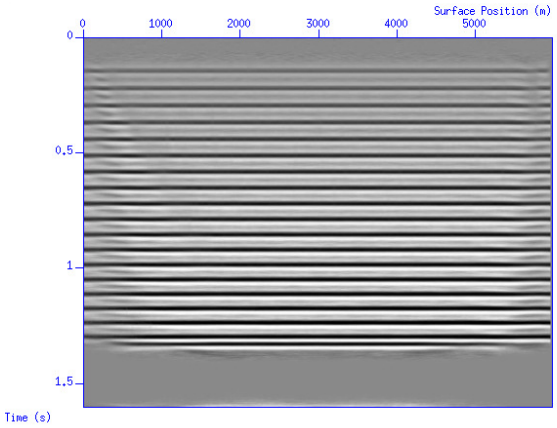

Figure 4: Example 1: Stacked image generated with weight function (3) (PIM, $\beta = \alpha$).

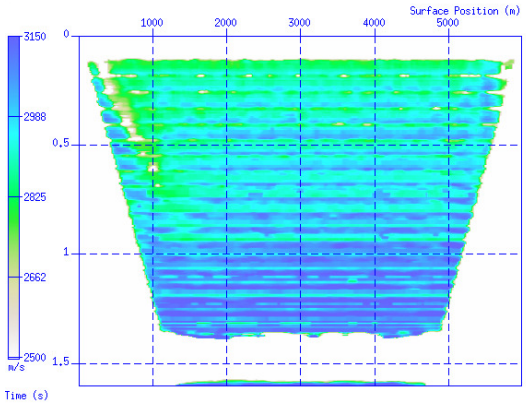

Figure 5: Example 1: Masked velocity map prior to B-spline interpolation.

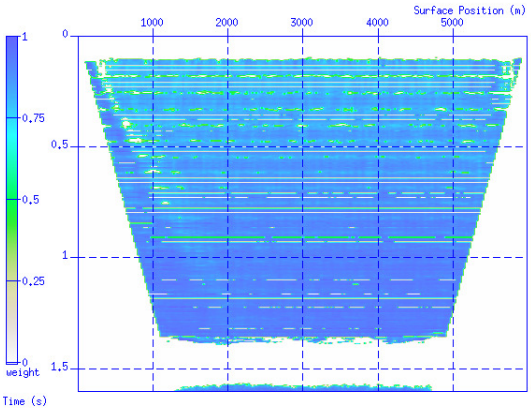

Figure 6: Example 1: Weight map obtained according to equation (12).

improved reflector images as compared to Figure 2, emphasizing the importance of the weight function in the stack.

Performing the image division under application of the stabilization and cleanup measures as described in the previous section, we obtain an intermediate velocity map (prior to the B-spline interpolation) and the weight map, corresponding to equations (5) and (12), respectively, shown in Figures 5 and 6. The intermediate velocity map already resembles the original model in the central area. We see that our cleanup procedure removes most of the velocities at shallow depths. At shallow depths, the velocities extracted by the original procedure are rather unreliable because of the short usable offset range. Moreover, we see in Figure 5 the effect of the trapezoid filter. The weight map shows that the extracted weight is high throughout the model, a good indication that the extracted velocities are consistent with the data.

By means of a B-spline interpolation, we fill the gaps in Figure 5 to obtain the final velocity model of MVA by DPIM (Figure 7). Note that the velocities below the deepest refletor have no physical meaning. They are simply obtained by B-spline extrapolation of the velocity information above. Above the deepest reflector, the velocity model acceptably resembles the input constant-gradient model of Figure 1.

Migrating the original data with this velocity model results in the migrated image displayed in Figure 8. We see that this migrated image is consistent with the image stack of Figure 2, except for the regions where missing illumination did not allow for velocity extraction.

To assess the quality of the velocity model, Figures 9a-d show four selected CIGs of the migrated image

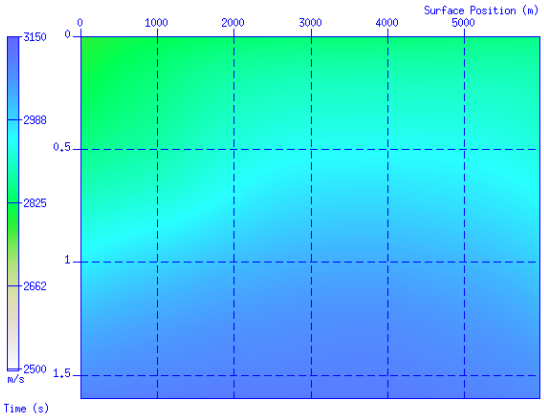

Figure 7: Example 1: Final velocity map after B-spline interpolation and smoothing.

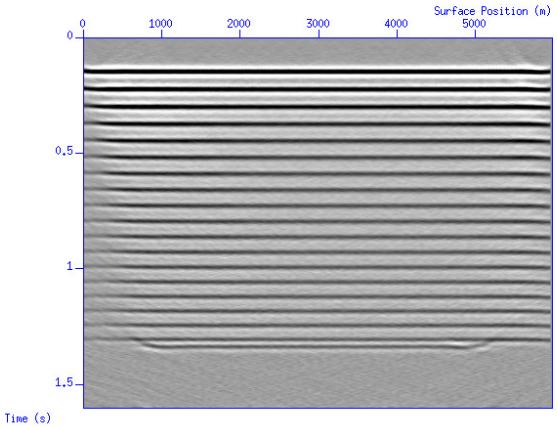

Figure 8: Example 1: Migrated image obtained using the final velocity map in Figure 7.

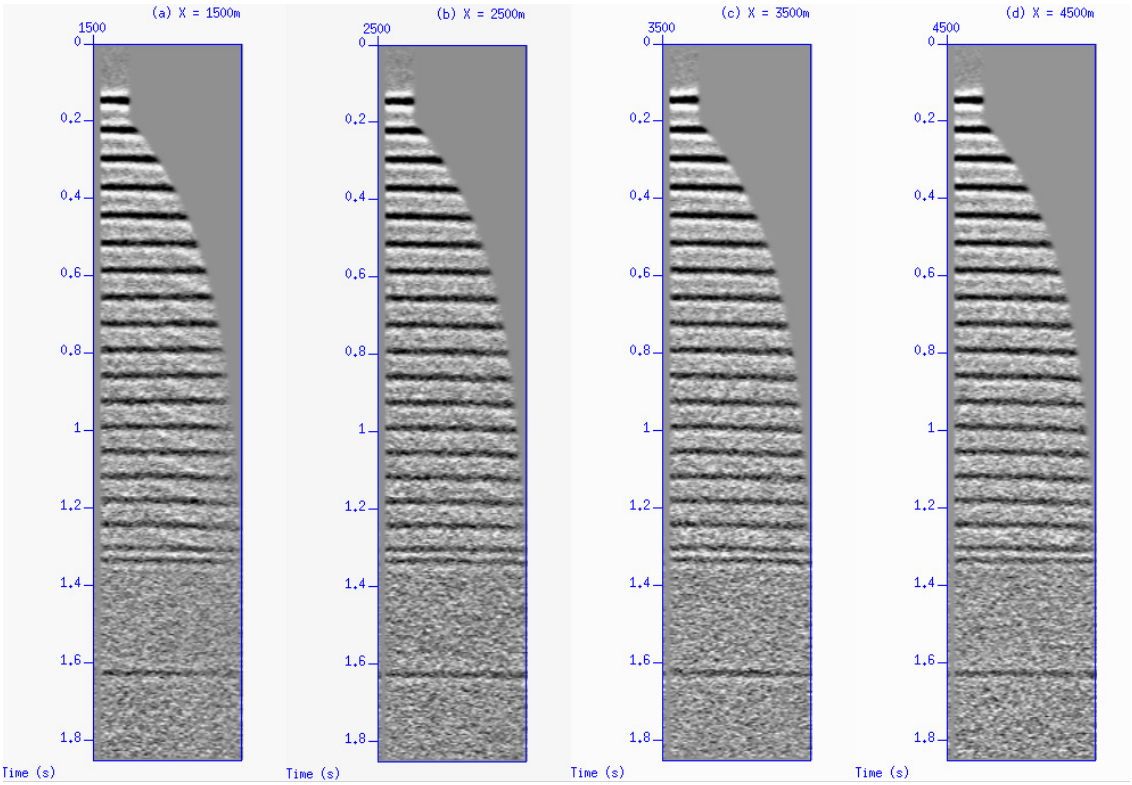

Figure 9: Example 1: Selected CIGs of the migrated data using the final velocity model. (a) $X = 1500$ m; (b) $X = 2500$ m; (c) $X = 3500$ m; (d) $X = 4500$ m.

in different parts of the model. We see that the events have been acceptably flattened all over the model. Some minor residual moveout could be corrected by conventional MVA.

Example 2: Nonvertical-gradient model

For the next tests, we used a model with the same reflectors as in Example 1, but with linear velocity variations in both the vertical and lateral directions. The variation in depth is the same as the in the previous

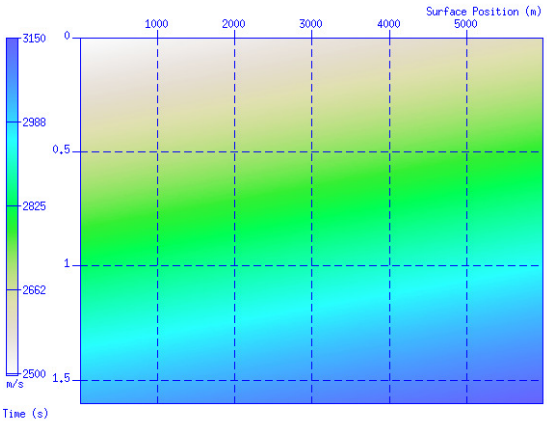

Figure 10: Example 2: Model with nonvertical gradient used to generate the synthetic data.

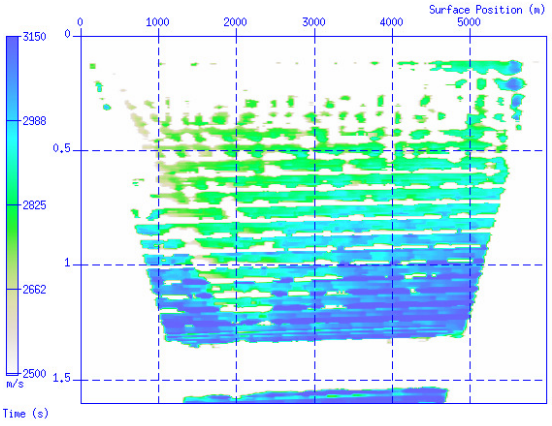

Figure 11: Example 2: Masked velocity map prior to B-spline interpolation.

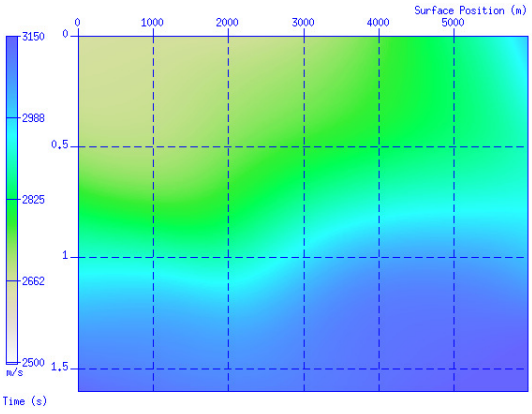

Figure 12: Example 2: Final velocity map after B-splines interpolation ans smoothing.

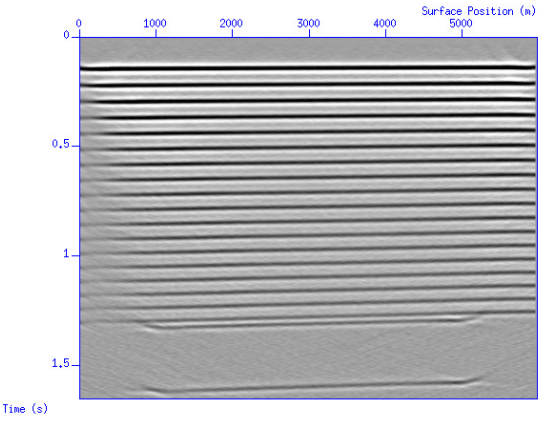

Figure 13: Example 2: Migrated image obtained using the final velocity map.

example (200 m/s for each 1000 m in depth) and the lateral variation is 20 m/s for each 1000 m to the right (see Figure 10). Thus, the velocity at the right extremity of the deepest reflector is 3600 m/s. All other parameters, i.e., the input set of velocities, wavelet, and signal-to-noise ratio, are the same as in Example 1.

Figure 11 shows the masked velocity map (before B-spline interpolation) for this example, and Figure 12 exhibits the final velocity model after interpolation and smoothing.

The migrated section obtained using this velocity model is displayed in in Figure 13 and some selected CIGs for these migrated data are shown in Figures 14a through 14d, respectively. We see that the lateral velocity variations introduce some errors in the extracted velocity model, but the overall result is still acceptable for a fully automated procedure. Again, the minor residual moveout in the CIGs could be corrected by conventional MVA.

Example 3: Low-noise scenario

In this test, we repeated the MVA of Example 1 with a different set of input velocities. It covers the same range from $v_{min} = 1200$ m/s to $v_{min} = 4000$ m/s, but now at a sampling rate of $\Delta v = 200$ m/s.

The main routine for generating the velocity map in Example 1 took about 55 minutes. The coarser sampling of the velocity space reduced the run time to 14 minutes. Figure 15 shows the resulting velocity map using this new set of velocities, and Figure 16 depicts the corresponding migrated section. We notice

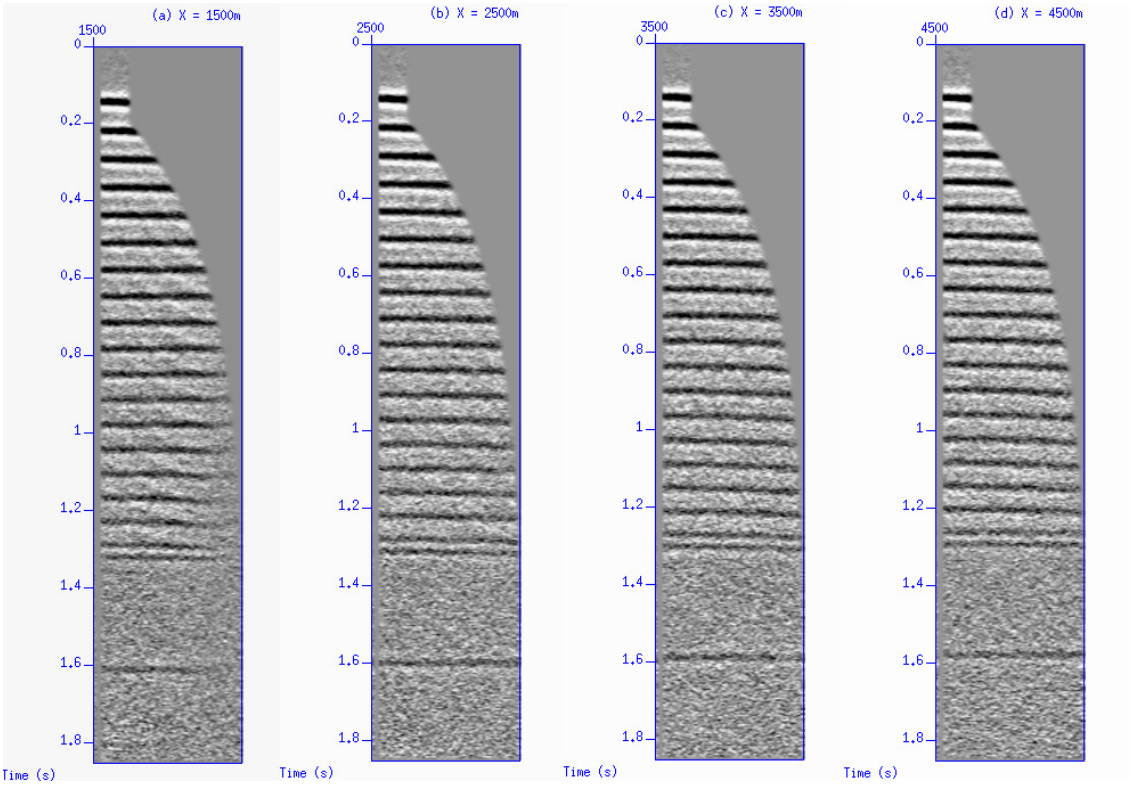

Figure 14: Example 2: Selected CIGs of the migrated data using the final velocity model. (a) $X = 1500$ m; (b) $X = 2500$ m; (c) $X = 3500$ m; (d) $X = 4500$ m.

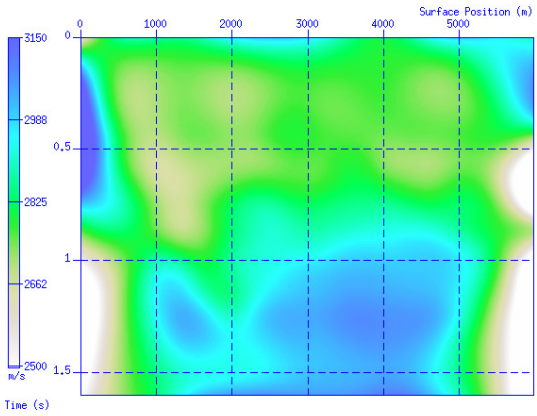

Figure 15: Example 3: Final velocity map. Compare to Figure 7.

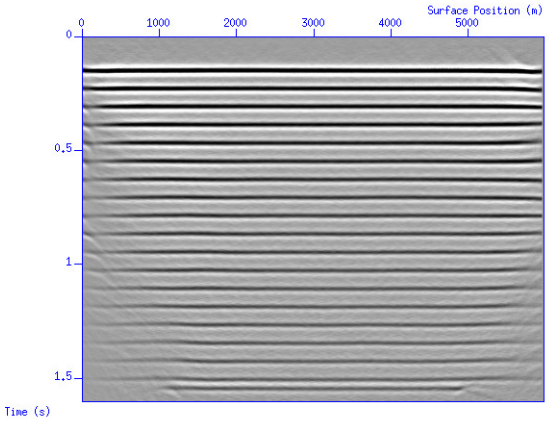

Figure 16: Example 3: Migrated image. Compare to Figure 8.

that the quality of the velocity model and migrated image remain practically inaltered, indicating that this coarser sampling of the velocity space is sufficient for this model. The possibility of a coarser sampling of the velocity space is a direct consequence of our more robust extraction procedure.

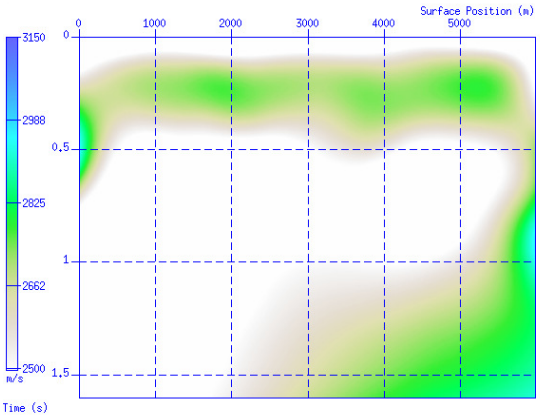

Figure 17: Example 4: Final velocity map. Compare to Figure 7.

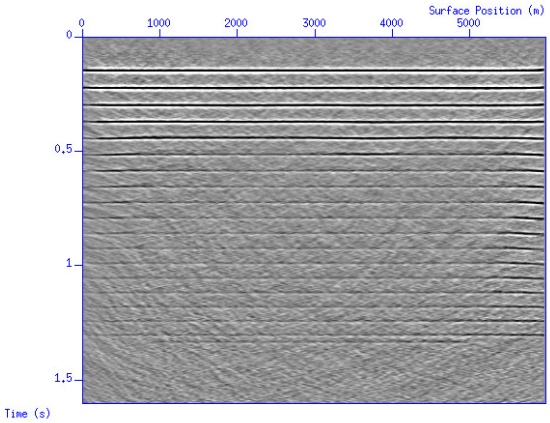

Figure 18: Example 4: Migrated image. Compare to Figure 8.

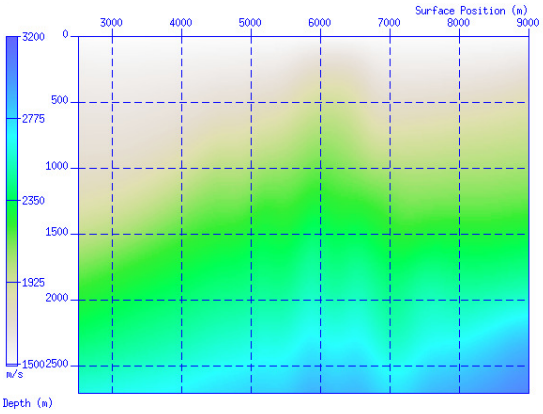

Figure 19: Example 5: Marmousoft model.

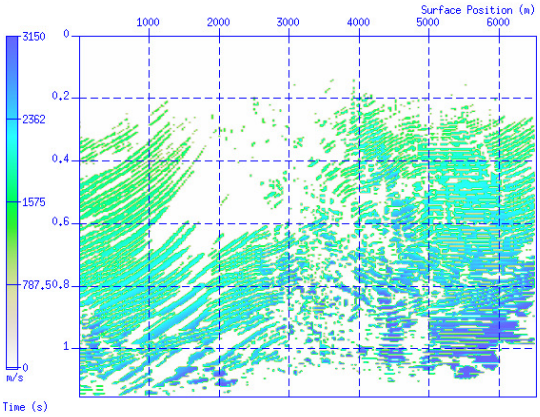

Figure 20: Example 5: Extracted velocity map.

Example 4: High-noise scenario

In the next test, we evaluated the effect of stronger random noise on the method. For this purpose, we decreased the signal-to-noise ratio in Example 1 to 5 and kept all other parameters as before.

Figure 17 shows the final velocity obtained in this scenario of higher random noise, and Figure 18 shows the final migrated section obtained with this velocity model. We see that the lower SNR leads to a lower quality of the recovered velocity model, particularly in the deeper part. This leads to a deteriorated image quality for the deeper reflectors. However, the positioning of the shallower reflectors in the migrated image is still acceptable.

Example 5: Marmousoft data

Our final example is a consistency test with the previous implementation of Schleicher and Costa (2009). We applied the current implementation to the same Marmousoft data set, simulated using Born modeling in a smoothed version of the Marmousi model (Billette et al., 2003). As a reference for the expected velocity range, Figure 19 shows the vertically converted rms-velocity model, and Figure 20 depicts the velocity values extracted by our robust masked division procedure.

The set of velocity models started at 1200 m/s and goes up to 4300 m/s, each new model increasing the constant velocity by 50 m/s. The runtime for the main routine for creating the velocity map was about 44 minutes. Figure 21 depicts the final velocity model, and Figure 22 shows the resulting migrated

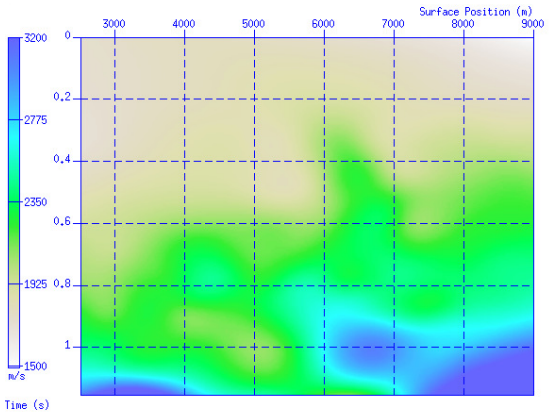

Figure 21: Example 5: Final velocity map after B-splines interpolation and smoothing.

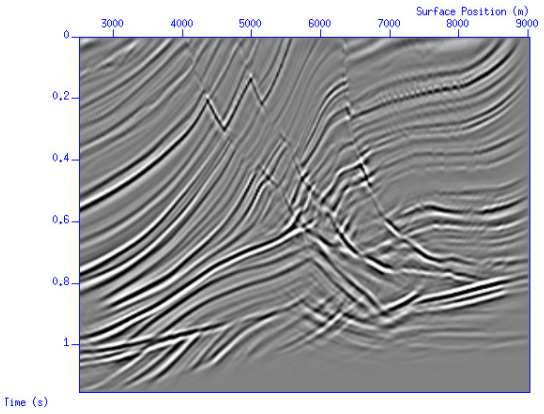

Figure 22: Example 5: Migrated image obtained using the final velocity map in Figure 21.

image. These images demonstrate that the current implementation has not lost quality over the original implementation of Schleicher and Costa (2009), who worked with a 25 m/s velocity interval.

DISCUSSION

In tests similar to Examples 1 through 4, we evaluated different situations in order to gauge the method's sensitivity to various cases of noise, variations of the velocity in the horizontal and vertical directions, wavelet signatures, and input set of models, among others. The main factors used in evaluating the results were:

- ability to differenciate signal from noise;
- time required to run the program;
- quality of the migrated image created by using the velocity model given by the method;
- flatness of the CIGs from this final migrated section.

Some observations from the results of these tests are:

- For data with a signal-to-noise ratio of 5 or lower, the method produced poor results.
- Having a set of velocities with twice the samples (increasing the velocity by 25 m/s for each new model) increases the processing time substantially (145% increase) but the quality of the resulting model and migrated section is similar. For simple models, even coarser velocity sampling is sufficient.
- Low-frequency data (simulated using Ricker wavelets with peak frequencies lower then 7.5 Hz) decrease the quality of the results.
- Horizontal velocity gradients higher than 20 m/s for each 1000 m can compromise the resulting velocity model.

There are several other parameters that could be altered in the method, which might help to improve the robustness of the velocity extraction or the quality of the results. Some of the properties of the procedures that were kept constant in this study but will be changed in future investigations are:

- The coherency measure used in the weight function (14): Other possibilities include regular semblance (Neidell, 1971) or some variation of it or a crosscorrelation function.

- The type of weight function itself (3): Here we used a real exponential function. Another possibility is a complex exponential, as in (Landa et al., 2006).
- The set of velocity models: It could include samples with varying velocities, or a combination of other different models, instead of only constant velocity models.
- The type and size of the window used in the coherency measure calculation.
- The criteria for accepting the image division values in equation (7).

CONCLUSIONS

This study develops on the work of Schleicher and Costa (2009) about performing Migration Velocity Analysis using path-summation imaging. We have tested the performance of the method under variation of several parameters and characteristics of the method. As a consequence, we can recommend some guidelines for implementing the method. Our numerical examples demonstrated the performance of this routine as a robust automatic tool for extracting an initial velocity model, at relatively low computer costs, with no previous knowlege of the subsurface model. Also, the examples and additional tests elaborated on the limitations of the current implementation of the method, such as a minimal signal-to-noise ratio and a maximal lateral velocity gradient.

ACKNOWLEDGMENTS

The authors would like to thank Professors Maria Amélia Novais Schleicher, Lúcio Tunes dos Santos and Ricardo Biloti, from the Group of Computational Geophysics of the State University of Campinas (DMA/IMECC) for fruitful discussions. We would also like to thank Petrobras (PRH-PB230), CNPq, and the sponsors of the WIT Consortium for the financial support.

REFERENCES

Berkhout, A. G. (2014). Review paper: An outlook on the future of seismic imaging, part III: Joint migration inversion. *Geophysical Prospecting*, 62(5):950–971.

Billette, F., Bégat, S. L., Podvin, P., and Lambaré, G. (2003). Practical aspects and applications of 2D sterotomography. *Geophysics*, 68:1008–1021.

Bleistein, N. (1987). On the imaging of reflectors in the earth. *Geophysics*, 52(7):931–942.

Clapp, R. G., Biondi, B., and Claerbout, J. F. (2004). Incorporating geologic information into reflection tomography. *Geophysics*, 69:533–546.

Costa, J. C. and Schleicher, J. (2011). Double path-integral migration velocity analysis: A real data example. *Journal of Geophysics and Engineering*, 8:154–161.

Erdélyi, A. (1956). *Asymptotic expansions*. Dover Publications.

Feynman, R. and Hibbs, A. R. (1965). *Quantum mechanics and path integrals*. McGraw Hill.

Keydar, S. (2004). Homeomorphic imaging using path integrals. In *66th Annual International Meeting*, page P078:1âĂŞ4. EAGE.

Landa, E. (2004). Imaging without a velocity model using path-summation approach. In *74th Annual International Meeting*, number Expanded Abstracts, pages 1818–1821. SEG.

Landa, E., Fomel, S., and Moser, T. J. (2006). Path-integral seismic imaging. *Geophysical Prospecting*, 74:491–503.

Neidell, N. S. e. M. T. T. (1971). Semblance and other coherency measures for multichannel data. *Geophysics*, 36:482–497.

Schleicher, J. and Costa, J. C. (2009). Migration velocity analysis by double path-integral migration. *Geophysics*, 74:WCA225–WCA231.

Schleicher, J., Costa, J. C., Santos, L. T., Novais, A., and Tygel, M. (2009). On the estimation of local slopes. *Geophysics*, 74(no. 4):P25âĂŞP33.

Tygel, M., Schleicher, J., Hubral, P., and Hanitzsch, C. (1993). Multiple weights in diffraction stack migration. *Geophysics*, 58:1820–1830.

Virieux, J. and Operto, S. (2009). An overview of full-waveform inversion in exploration geophysics. *Geophysics*, 74:WCC1–WCC26.